RESEARCH ARTICLE

Design of a wheeled wall climbing robot based on the performance of bio-inspired dry adhesive material

Hongkai Li[1,2]* , Xianfei Sun[3], Zishuo Chen[1], Lei Zhang[1], Hongchao Wang[3] and Xing Wu[1]

[1]College of Mechanical and Electrical Engineering, Nanjing University of Aeronautics and Astronautics, Nanjing 210016, China [2]Science and Technology on Electro-optic Control Laboratory, Luoyang 471000, China and [3]College of Astronautics, Nanjing University of Aeronautics and Astronautics, Nanjing 210016, China
*Corresponding author. Email: hklee@nuaa.edu.cn

Abstract

Inspired by gecko's adhesive feet, a wheeled wall climbing robot is designed in this paper with the synchronized gears and belt system acting as the wheels by considering both motion efficiency and adhesive capability. Adhesion of wheels is obtained by the bio-inspired adhesive material wrapping on the outer surface of wheels. A ducted fan mounted on the back of the robot supplies thrust force for the adhesive material to generate normal and shear adhesion force whilemoving on vertical surfaces. Experimental verification of robot climbing on vertical flat surface was carried out. The stability and the effect of structure design parameters were analyzed.

1. Introduction

With the development of robotic technology, robots have been employed for decades to keep humans away from dangerous tasks and areas. Climbing is one of the most dangerous tasks for humans, and thus, wall climbing robots, as a branch of specialized robots, is expected to be adopted in place of humans for inspection of nuclear power plants and petrochemical industry [1, 2, 3].

One of the main considerations of wall climbing robot is adhesion capability, which can dominate the robot adaptability and maximum payload. Vacuum suction, magnet adhesion, and grasping by claws are widely used as adhesion methods. Vacuum suckers are mainly used to generate adsorption. To align the sucker to working surface of robot structure, different walking mechanisms and control method are proposed. Zhu et al.4 proposed a biped wall climbing robot, in which the posture and alignment were precisely controlled to generate enough adsorption. Yanagida et al. [5] designed a quadruped robot with fours inglejoint bent leg. The wall climbing capability was achieved using micro-suction cups from air stick that has thousands of microscopic air pockets to create partial vacuums between the tape and target surface. To achieve the functions like many little suckers or micro-suction cups for wall climbing robot systems, impeller-type adhesion mechanism was also designed by Koo et al. [6] The attachment of vacuum suction can be very strong and robust, [7, 8] but it is only suitable to be used on relatively flat substrate without obstacles. Besides, the motion speed of robot is limited due to time consumption of vacuuming air to generate enough adhesion forces. Magnetic adhesion has been implemented in wall climbing robots for specific applications such as nuclear facilities inspection [9, 10]. Grasping by claws is an excellent bio-inspiration and is widely adopted by insects and animals. Most of the claws rely on spine mechanisms, [11] such as passive spine gripper7 and RiSE micro-spines [12]. It is known that robots with vacuum suctions and magnet adhesions are time-consuming in working and available for the specific moving surface. The robots with the grasping technique can climb on rough surfaces like brick and stone, but the method cannot be applied on the smooth and flat surfaces.
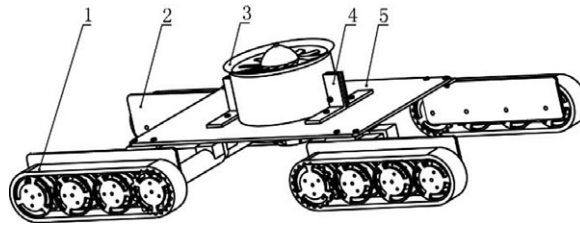
Figure 1. *Structure of the wall climbing robot. Label 1 represents the robot adhesive wheel; label 2 and 5 denote the different parts of robot frame; label 3 indicates a ducted fan, and label 4 presents the fixture.*

The natural adhesive pads from geckos, crickets, ants, and some arthropods like stick insects exhibit strong climbing ability regardless of the roughness of the contact surface. Therefore, the design of an adhesive mechanism for a climbing robot based on insect techniques has considerable merits, which is an attractive method for wall climbing robots as well. Adhesion includes wet and dry adhesion mechanism. Inspired by the remarkable locomotion performance of arthropods like stick insects climbing vertical surfaces with their wet adhesion pads, a wet adhesion-inspired bionic climbing robot with six adhesion pads was designed. Experiments showed that the robot has good performance moving on vertical substrates even though limited in the wet contact situations [13].

Learned from the excellent adhesion capability of gecko's seta, several sorts of bio-inspired adhesive material were developed, such as polyvinyl siloxane [14] and carbon nanotube array [15]. These advanced materials provide an opportunity for the robot to move like the wall climbing animals [16]. Gecko inspired dry adhesion based on micro-nanoscale hierarchical arrays were especially concerned for application in climbing devices [17]. With the inspirations of caterpillars locomotion strategy, Han et al. [18] designed a miniaturized wall climbing segment robot, which consists of seven gecko-inspired adhesive pads that fabricated from polydimethylsiloxane (PDMS) with the area of 20 mm × 10 mm. Peyvandi et al. [19] designed a self-loading locomotion mechanism for wall climbing robots, which employed four rectangle wheels with adhesive material on the surface. Liu et al. [20] designed a new wall climbing robot platform that could move on the vertical surface with various curvatures, and the robot has eight footpads whose locomotion was achieved by asymmetric compliant four-bar mechanism. In addition, a tail was implemented at the end of the robot to reduce the pitch-back moment. Some quadruped robots with dry adhesive pad also had the ability of water repellency [21]. Leg mechanisms were mainly used for wall climbing robot that adopt dry adhesion characteristics. The adhesive state must be examined in each step to keep it steadily attached on the wall, but this imposes restrictions on the motion speed.

As a systematic issue, the adhesion ability of wall climbing robot depends on both performance of adhesive material and structure design. In this paper, a wheeled wall climbing robot is proposed to climb on the flat surface with different materials. Track wheels with dry adhesive material wrapped outside are employed to provide adhesive force. The rest of this paper is organized as follows. Section 2 depicts the structural design of the wall climbing robot. Section 3 elaborates on the modeling and analysis of thrust force and adhesion material, and Section 4 discusses the adhesion performance of the adhesive material and robot motion. Finally, Section 5 provides conclusions of the current work.

2. Structural design of the wall climbing robot

The wall climbing robot is designed with the utilization of adhesive material. The 3D model is shown in Fig. 1, in which each element is labeled with a different number. Four adhesive wheels (label 1) are placed on the corners of the robot symmetrically. Four robot wheels and ducted fan (label 3) are installed on the different parts of robot frame (label 2 and label 5). The ducted fan offers thrust force for the robot during moving. And the fixture (label 4) is used to hold the ducted fan onto the robot back.
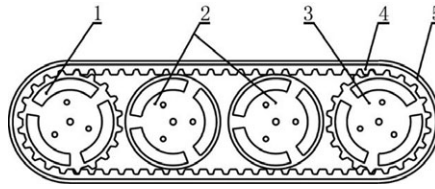
Figure 2. *Structure of adhesive wheel. Label 1 indicates the driving wheel, label 2 indicates the induction wheels, label 3 represents the towing wheel, and the label 4 represents the synchronous pulley and labelled with number 5 denotes the adhesive material belt.*

Motion mechanism is critical for most robots, and it also applies for wheeled wall climbing robots. To enhance the adhesive force by increasing the contact area, the mechanism of crawler wheel structure is used as a prototype. Different from the rough outer of crawler belt which is used to increase friction with road, the outer of wheels for the wall climbing robot is replaced by synchronous belt not only to increase the contact area with the substrate, but also to facilitate the installation of adhesive material on the wheel firmly. The structure of the adhesive wheel is shown in Fig. 2. Two synchronous gears are employed as the driving and towing wheel (label 1 and 3) instead of using crawler wheels. The adhesive material belt (label 5) is adhered directly to the surface of synchronous belt (label 4) with the adhesive function surface outside. Two induction wheels (label 2) are used to flatten the belt to increase contact area in moving on vertical surface.

Each driving wheel is actuated by one DC motor. The total output torques of four motors must overcome the torques that derived from the gravity and peeling forces practically when the robot moving up on vertical surface, which means,

$$4\frac{\tau}{r} > \left(M + \sum_{i=1}^{4} m_i\right) g + \sum_{i=1}^{4} f_i \qquad i = 1...4 \tag{1}$$

where τ is the output torque of each motor, r is the radius of the driving wheels, and m_i and f_i are the weight and peeling force of each wheel, respectively.

In Eq. (1), r denotes the distance between the motor axle and moving surface in actual. The thickness of belt and adhesive material is neglected because of the small value relative to the radius of the wheels. The DC motor working at 24 V is selected with the no load speed of 10,700 r/min with the reduction ratio of 1:252. Normal torque and stall torque are 14 and 57 kg·cm, and the corresponding no load and stall current are 10 and 300 mA, respectively.

3. Modeling and Analysis

3.1. Modeling of wall climbing

The wall climbing robot is modeled by a planar multi-rigid body adhered on vertical substrate with the effect of normal force, as shown in Fig. 3. The planar model is mainly composed of the front and rear crawler-like wheels, robot body, and a ducted fan.

In Fig. 3(a), l is the length between the center of front and rear tack wheels, n is the half-length of a track wheel, B is position the CoM (Center of Mass) of robot body excluding all the wheels, h is the length between CoM and contact surface, and r is half-height of tack wheels. Figure 3(b) showed the free body diagram of wall climbing robot in steady equilibrium, in which F_1 and F_2 are the shear adhesion forces generated by the adhesive material on the wheels; f_1 and f_2 are the peeling resistance forces; m and M are the mass of wheels and robot body, respectively; g is the gravitational acceleration; N_1 and N_2 are reaction forces of wall to front and rear wheels; N denotes the thrust force executed by ducted fun; τ_1 and τ_2 are the torques of front and rear motors, respectively; τ is the torque generated by the peeling force. Normally, the peeling force is very small so the τ is neglected. Equations (2) and (3) can
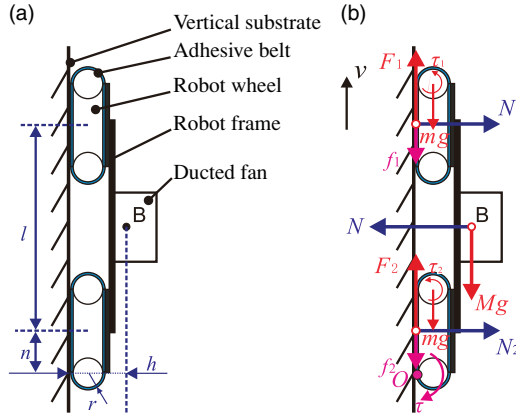
Figure 3. *Diagram of robot planar model for analysis. (a) The planar model of the wall climbing robot. (b) The free body diagram.*

be obtained in vertical and horizontal direction, respectively,

$$F_1 + F_2 = f_1 + f_2 + (M + 2m)g \tag{2}$$

$$N_1 + N_2 = N \tag{3}$$

The torque equilibrium equation is derived assuming the robot has the trend to turn around point O,

$$N\left(\frac{l}{2} + n\right) - N_1(l + n) - N_2 n = 4mgr + Mgh \tag{4}$$

By combining Eqs. (3) and (4), the following relationship can be derived:

$$(N - 2N_1)\frac{l}{2} = 4mgr + Mgh \tag{5}$$

There are two cases for thrust force of N with different reaction force:

Case 1: The value of reaction force N_1 is zero. A preload (thrust force) is imposed on the robot to generate enough shear force to hang the robot in vertical direction and adhesive force to adhere robot to the wall in the horizontal direction. Then the preload is decreased until reaction force N_1 become zero. In this case, the normal reaction forces are replaced by the adhesive forces, as shown in Fig. 4, in which α is the peeling angle between the wheel and the contact substrate, and F_{a1} and F_{a2} are the adhesive forces generated by the adhesive wheels, respectively. N_r is the support reaction force.

Hence, by considering the length of the wheels, Eq. (4) is transformed to the following:

$$N\left(\frac{l}{2} + n\right) + F_{a1}(l + n) + F_{a2}n = 4mgr + Mgh \tag{6}$$

And the below relationship is satisfied:

$$N + F_{a1} + F_{a2} = N_r \tag{7}$$

If F_{a1} and F_{a2} are large enough to avoid the overturn of robot, N can be zero ideally. Because of existence of the peel angle22 between the wheels and vertical substrate caused by the round wheels, the adhesive forces would gradually become smaller with the participation of new contact area and absence of the thrust force.

Case 2: The value of reaction forces are not zero (Fig. 3(b)). In this case, the thrust force N is used not only to overcome the turning torque of the weight of robot, but also to support extra normal pressure
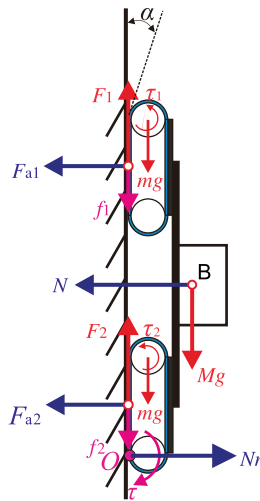
Figure 4. *Free body diagram of robot when reaction forces are replaced by adhesive forces.*
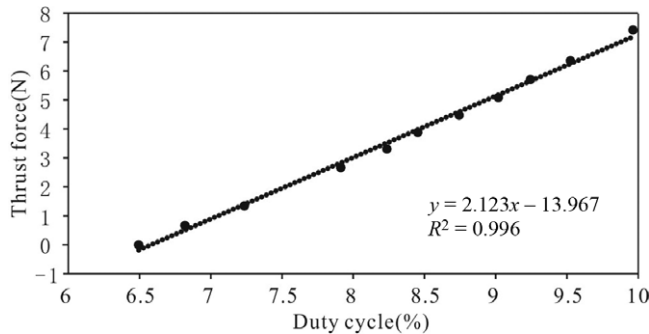

Figure 5. *Relationship between output thrust force and duty cycle of control signal.*

force for robot to generate shear adhesion force to hang the robot on the vertical substrate during moving. It is apparent that Case 2 would be a robust and safer choice for the adhesive wall climbing robot.

3.2. *Thrust force of the ducted fan*

Ducted fan used in adhesive robot is to generate positive force to push the robot toward the contact substrate and provide pressure for the adhesive wheels.

The ducted fan selected for the robot is actuated by a DC motor and can be regulated by a joystick with the 2.4-GHz remote controller with the weight of 580 g and diameter of 105 mm. Calibration of thrust was carried out using four digital scales that were placed on a chair with the same height. A wood board was used to block the inlet to simulate the contact substrate. Each wheel was put on a single scale. The ducted fan was controlled by joystick and the duty cycle of control signals and all the values of four scales were recorded to get the relation between output thrust force and duty cycle. Thrust force was computed by subtracting the weight of robot from the sum of all the recorded force values. An oscilloscope was connected to the input signal of motor to test the duty cycle of pulse width modulation. The frequency of control signal was set at 54 Hz. The duty cycle was limited to 10% in order to keep the output current in the secure range. The test results are shown in Fig. 5.
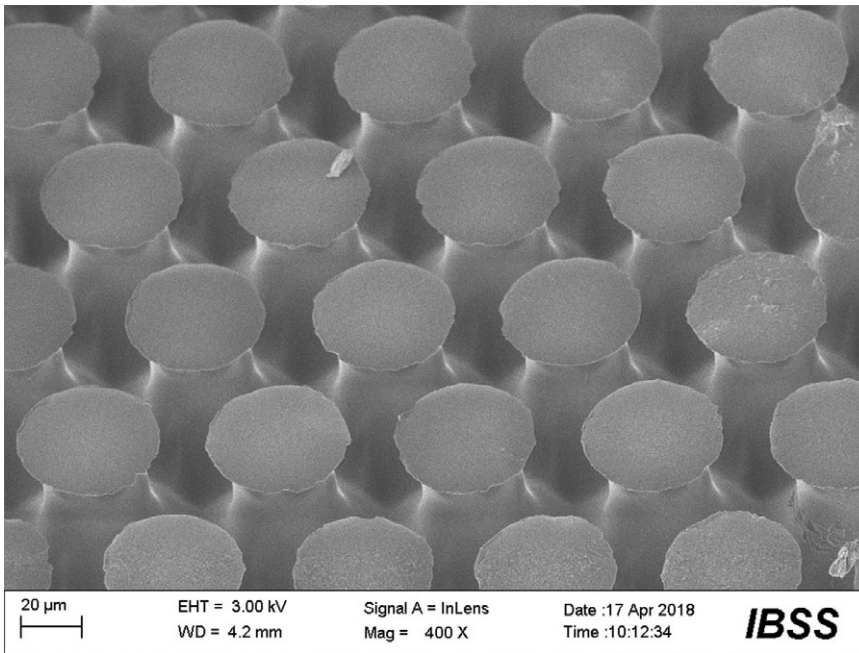
Figure 6. *Structure of the adhesive material.*

The equation of dash line is fitted and shown below:

$$F_t = 2.123 Duty - 13.97 \tag{8}$$

where F_t is the thrust force and *Duty* is the duty cycle of input signal. The goodness of fit R^2 is 0.996. The result shows that the thrust force can be thought as the linear function of duty cycle.

3.3. Determination of adhesive material size on the wheels

3.3.1. Relationship between shear adhesion strength and normal pressure

The size of the adhesive material stuck on the wheel is determined by both the thrust force and the weight of robot. The relationship between the norm pressure imposed on the material and the shear adhesion force was investigated in this section.

The used adhesive material is a bio-inspired structure mimicking seta hairs on gecko's feet and was fabricated by pouring two-compound polymerizing polyvinylsiloxane (PVS) into the holed template lying on a smooth glass support at room temperature. Prospective height of specimen was defined by spacers between the support and a covering flat surface that was used to squeeze superfluous polymer out of the gap. The ready-to-use cast was removed from the template after polymerization. The backside of the fibrillar casts was used for flat specimens. The material has excellent adhesion adaptability on relative flat surface. The structure and size are shown in Fig. 6. This adhesive consists of mushroom-shaped pillars [23] of about 100 μm in length, and bottom diameter of the support rod is 60 μm. The diameter of the end mushroom head is 40 μm.

The investigation was carried out on a home-made tribometer, as shown in Fig. 7. A two-dimensional force sensor was installed on the base plate of the tribometer, which can be controlled to move on both horizontal and vertical directions. The range of the force sensor was 10 N in two directions. The motion of the base plate was controlled by two step motors in the orthogonal directions. A closed-loop control algorithms for force and displacement were executed in the on-board computer. The control signals were

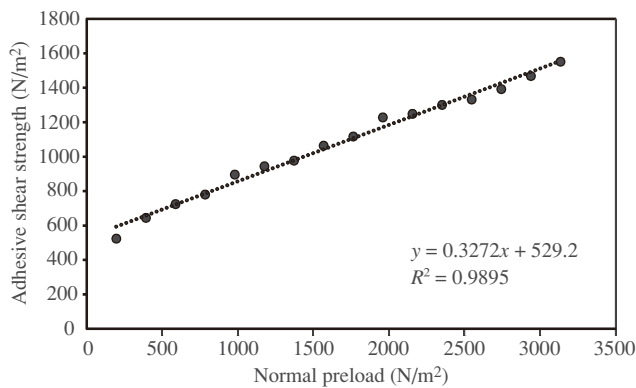**Figure 7.** *The home-made tribometer for adhesive material test.*

Figure 8. *Relationship between the normal pressure and the shear adhesion strength.*

sent to a driving board to manipulate the motors. A data collection board was employed to collect and transfer the force data to computer for further analysis.

The adhesive material was trimmed to size of 5 mm × 5 mm for the test and attached on the sensor with the functional surface toward a flat glass that fixed on the machine. The motor in vertical direction was controlled to move down until normal pressure reaches the set value and kept constant during each test. Then the sensor was actuated to move in horizontal direction until the material detaches from the contact substrate. The peak value of the recorded shear adhesion force data was recorded and considered as the maximum shear adhesion strength.

There are 16 different forces were tested in total with the normal pressure ranged from 196 to 3136 N/m^2. The shear adhesion strength increased from 524 to 1552 N/m^2, the data of which are shown in Fig. 8, The dash line is the fitted trend line of the discrete test points with the equation:

$$P_s = 0.3272P_n + 529.2 \tag{9}$$

where P_s is the shear adhesion strength and P_n is the normal pressure, with the unit of N/m^2.

The relation between the shear adhesion strength and normal pressure can be thought as linearity. Based on this equation, the size of material needed to maintain the robot moving on vertical surface can be evaluated, thus that the pre-pressure can be estimated for a certain output shear adhesion force.

3.3.2. Determination of adhesive material size on wheels

The priority is given to the shear adhesion force to determine the size of adhesive material required by the robot. By multiplying the contact area on both sides of Eq. (9), the relationship between shear adhesion force and size of contact area can be obtained for a given thrust force:

$$F_s = 0.3272F_n + 529.2S \tag{10}$$

where F_s is the shear adhesion force, F_n is the normal force act on the adhesive material, and S is the size of contact area.

The total weight of the robot is about 48.31 N excluding the adhesive material. According to Eq. (8), given the ducted fan works with the duty cycle of 10%, the output thrust force can reach 7.4 N. For the static case of robot hanging on the vertical substrate, the gravity of robot was overcome by shear force only, so the shear adhesion F_s of 48.31 N is required. Assuming that the maximum normal force is 7.4 N, then the contact area of 867.13 mm^2 is needed.

The type of 5M synchronous belts with 25 mm in width was selected as the transfer belt of the wheels, and the circumference was 160 mm. The length between the driving and towing gears was about 70 mm, thus the working area that contacts with the substrate was about 70 mm × 25 mm. As a result, the total contact area of four wheels is 7000 mm^2 (280 mm × 25 mm), which was greater than the required area by considering the ratio of effective contact area. According to Eq. (5), it can be verified that the torque condition can be satisfied for the given thrust force.

4. Results and Discussions

4.1. Shear adhesion and peeling force test of robot

Shear adhesion force and peeling force are most important for the wall climbing robot. The former will affect the adhesion performance with certain normal thrust of the ducted fan, while a small peeling force will decrease requirement of motor power.

A one-dimensional force sensor was used to test the shear adhesion force. Two ropes were used to hang the robot. One was tied between robot and sensor, and the other was tied to the sensor which was pull up to measure the maxim shear adhesion force. Because the thrust force was related to the duty cycle of control signal ducted fan, an oscilloscope was connected to the control board to measure the duty cycle of control signals which can be adjusted by the a joystick. After turning on the ducted fan, robot was pushed to adhere to the flat vertical substrate by the thrust force, then the rope was dragged until the robot had the trend to relax relative to the contact substrate. The net shear adhesion force was calculated by subtracting the gravity of robot from the obtained maximum sensor force. The test system is shown in Fig. 9.

The regression curve between the duty cycle and net adhesive shear force is shown in Fig. 10, in which the dash line denotes the trend line, the resulted relation is

$$F_A = 11.245D - 62.04 \tag{11}$$

where F_A is the shear adhesion force and D is the duty cycle of control signal. The goodness of fit is 0.9943 which indicates that the line can fit the discrete points well.

It can be seen from the figure that the shear adhesion force of wheels ranged from 16.35 to 50.82 N with the duty cycle of the control signal from 6.8 to 10%.

Peeling force is another vital factor that affects the motion performance of wall climbing robot. Based on the previous experiment, the adhesive force of this kind of bio-inspired adhesive material increases
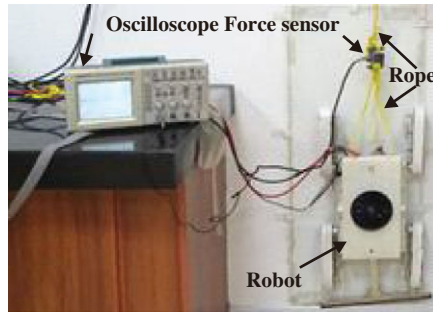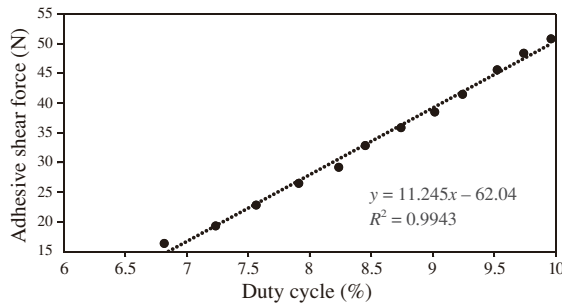
Figure 9. *Share adhesion force test of robot.*

Figure 10. *Relationship between duty cycle and shear adhesion force of robot.*

with the normal adhesive force in a certain range, whereas the force required to peel from the substrate is variable with the peeling angle [24], and the peeling strength was carried out by the following expression:

$$\left(\frac{F}{b}\right)^2 \frac{1}{2Ed} + \left(\frac{F}{b}\right)(1 - cos\Theta) - R = 0 \tag{12}$$

where F is the peeling force, d is the thickness of the adhesive tape, b is the width of the tape; E is the Young's modulus of the tape material, Θ is the peeling angle, and R is the energy required to fracture a unit area of interface [25].

According to the results obtained by outgroup in the previous experiments [26], the peeling force was about 1.31 N/cm, and the force was not sensitive to the peeling speed and the peeling angle. The peeling force of about 3.28 N was estimated for each wheel to detach from the contact substrate, which was negligible for the robot.

4.2. Experiment of robot moving on vertical substrate

The control system of the robot includes two parts to adjust the duty cycle of ducted fan and the motion of motors, respectively. The control diagram is shown in Fig. 11. The motion speed of robot was controlled by a joystick, the command was sent to robot by wireless communication. PD controller was used for each DC motor. The ducted fan was controlled by an independent controller. An inclinometer was adopted to detect the inclination of robot and compared with 0 degree, and the error was sent to a PD controller for the regulation of the duty cycle of ducted fan.

The experiment was carried out by controlling robot moving upward on a vertical flat Perspex sheet which was attached on the lateral board of an iron cabinet. A looped rope was tied to the robot to protect it during the experiment. Two electric wires were lead out and connected to the battery. The scenarios of the motion experiment were shown in Fig. 12. According to the results, the robot could still move
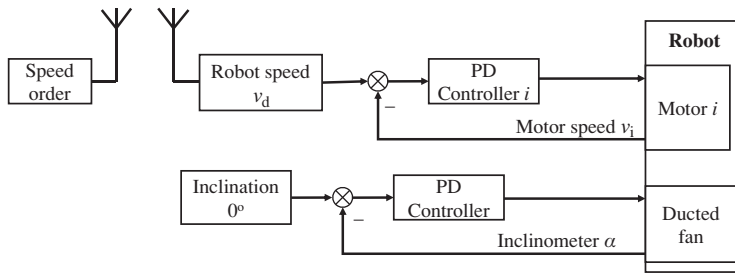
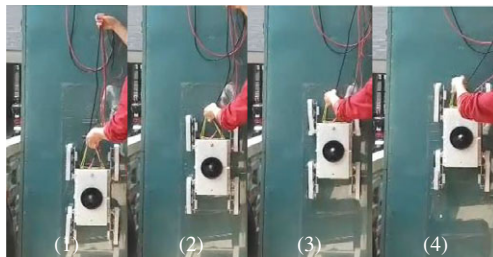**Figure 11.** *Robot control system diagram.*

Figure 12. *Scenarios of robot climbing on vertical substrate.*

successfully at the speed of 12 cm/s, though the duty cycle of the control signal for ducted fan was limited below 10% to protect the power amplifier.

4.3. *Stability when adhering on the vertical substrate*

4.3.1. *Static stability when adhering on the vertical substrate*

The stability issues of wall climbing robot includes lateral overturning and vertical sliding. In the lateral direction, robot has the trend of turning over around the lowest support point, while in the vertical direction, robot would slide downward if there was not adequate shear adhesion force.

The normal adhesion force between wall climbing robot and substrate can be huge even with little preload if the peeling angle was inexistent. According to the experiments on the sample material with the size of 5 mm × 5 mm, the normal adhesive force can reach 5.34 N with a preload of 3 N. In contrast, the material would detach from the substrate easily under small peeling angles. The bio-inspired adhesion material has the similar detachment characters with the animal gecko, which was also discussed elsewhere [22].

When robot stops moving and adheres on the vertical substrate, as shown in Fig. 13(a), the boundary conditions can be predicted by Eqs. (2) and (6). The shear and normal adhesion forces are normally enough to satisfy the above condition even withdrawing the normal pressure according to the result in Fig. 8.

This case happens when robot stops moving on the vertical substrate. And the conditions can be easily satisfied on behalf of the excellent performance of the adhesive material.

4.3.2. *Dynamic stability during moving*

In vertical direction, dynamic stability is mainly concerned on sliding down and turning over during moving. Sliding down will happen when the shear adhesive force is insufficient. It is affected not only by the thrust force but also by the cleanness of adhesive material and the motion coordination between the front and rear wheels. Unlike the self-cleanness ability of animal's feet, this character of the adhesive
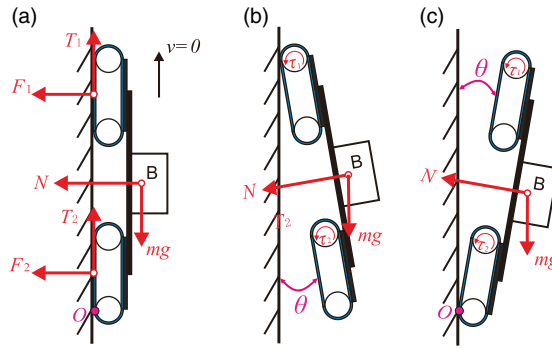
Figure 13. *Static stability and failure cases. (a) The static state; (b) the case peeling from rear wheels; and (c) the case peeling from front wheels.*

material is still under research and cannot be controlled at present. Therefore, the thrust force is the only controllable variable for it.

The thrust force is controlled by adjusting the duty cycle according to the error between inclination angle of robot and the setting angle of 0 degree. In the previous test results, it can be found that the performance of the bio-inspired adhesive material has excellent normal and shear adhesion strength with small preload. The required thrust force can always be satisfied to avoid the sliding down when moving on relative clean substrate.

Caused by the incoordination between the front and rear wheels, the inner force will also result to sliding and turning over, which affects the adhesion performance of robot.

Theoretically, turning over would happen around the fore or the rear supporting point, as shown in Fig. 13(b) and (c). In Fig. 13(b), the rear wheels detach from the vertical substrate and the robot turns around the fore support point. However, for the wall climbing robot, it would occur when the output torque of rear wheels is greater than that of front ones, meanwhile, the front wheels keep attached. In application, the front and rear wheels nearly have the same adhesion performance, if the ducted fan is installed on the center of the robot, the thrust force will be assigned on the front and rear wheels equally. Because of the gravity, the normal pressure on the front wheels is actually smaller than that on the rear wheels, and therefore the smaller adhesion force. Practically, this case would not occur unless the adhesion of rear wheels lost efficacy.

The most possible failure case for wall climbing robot is to turn over around the rear support point, as shown in Fig. 13(c). There is a natural peeling angle between the wheels and contact substrate because of the semicircle in the front part of the wheels. Assuming that the inclination angle between robot and vertical substrate is θ, according to Eq. (6), the total turning torque in the right part can be derived that,

$$\sum T = 2mg(r\cos\theta + n\sin\theta) + 2mg(r\cos\theta + (l+n)\sin\theta) \\ + Mg(r\cos\theta + (h-r)\sin\theta) \quad (13)$$

where $m = 600$ g, $M = 2380$ g, $r = 29$ mm, $l = 368$ mm, and $n = 73$ mm. By neglecting the radius of motor for the supporting torque of ducted fan, and considering the worst condition that the adhesive material is wrapped on the rigid wheels without elasticity, the total thrust force required to balance the turning torque can be obtained as:

$$N = \sum T / l \quad (14)$$

and the relationship between the inclination angle and the required thrust force is shown in Fig. 14.

In Fig. 14, it can be found that the thrust force of ducted fan needed to balance the turning torque of the robot is nearly linear to the inclination angle of robot in the range of 0–40 degrees. This implies that
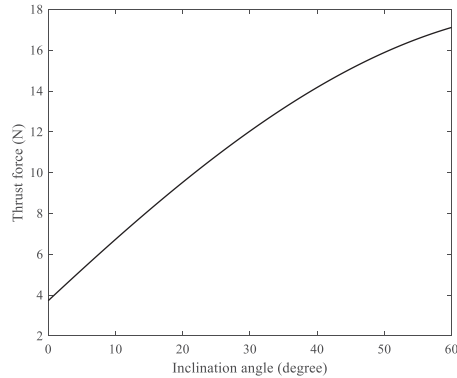
Figure 14. *Thrust force required to balance the turning torque with the change of inclination angle.*

a rapid adjustment of duty cycle of ducted fan is required to push the robot back to the vertical substrate at the beginning of inclining.

4.4. *Effect of robot structure on wall climbing performance*

Supposing the inclination angle is determined, and the overturning torque of robot of a function of the size and weight of robot according to Eq. (13). To avoid the overturning of robot, one way is to lower the overturning torque, another is to increase the thrust force to overcome the overturning.

According to Eq. (13) and the values of robot size and weight of each part, the ducted fan is the main contributor to the total torque because of the large mass and long force arm relative to the other parts. An effective way is to decrease the height of CoM to lower overturning torque once the ducted fan was selected. The air inlet of the ducted fan is a key factor for the output thrust force. A broad and long air inlet is required if bigger thrust force is expected, while a lower position of the ducted fan will decrease the airflow. So a trade-off must be made between the position of fan and the thrust force.

In Eq. (14), the required thrust force to balance the overturning torque will decrease with the increase of l. To lower the requirement of output thrust force, a long distance between the position of ducted fan and supporting point of robot is necessary, but if the position of fan is beyond the front wheels, it will decrease the normal pressure on rear wheel due to the see-saw phenomenon around front wheel.

The attachment characters of the bio-inspired adhesive material pay a vital role on the performance of wall climbing robot. Gecko setae are a non-lubricated adhesive system based on van der Waals forces [27]. Inspired by this principle, this biomimetic material has strong adhesive forces both in shear and normal directions with small pre-pressure. It would be also easily detached from the contact substrate with a little peeling angle [22]. According to Fig. 8, a small preload will cause a great adhesive shear strength, and the shear strength is nearly a linear relationship with the pressure in a certain range. For the large area application on robot, increasing available contact area with the substrate becomes an important factor that needs to be considered in practice. In this design, it was improved by adding a thick soft elastic material between the adhesive material and the rigid wheels surface.

5. Conclusion

In this paper, a wheeled wall climbing robot with bio-inspired material is proposed which can move faster than the legged one. The modeling and analysis of wall climbing robot utilizing adhesive material were provided. The robot was designed specifically based on the experiment results of adhesive material and ducted fan. Furthermore, the force character of the robot was tested, and the wall climbing experiment was carried out on a flat vertical surface. The static and dynamic stability, together with the effect of structure on wall climbing robot performance, were discussed and confirmed the reliability of the design.

References

[1] M. A. S. Teixeira, H. B. Santos, N. Dalmedico, L. V. R. de Arruda, F. Neves-Jr. and A. S. de Oliveira, "Intelligent environment recognition and prediction for NDT inspection through autonomous climbing robot," *J. Intell. Rob. Syst.* **92**, 323–342 (2018).

[2] H. B. Santos, M. A. S. Teixeira, A. S. de Oliveira, L. V. R. de Arruda and F. Neves-Jr., "Quasi-omnidirectional fuzzy control of a climbing robot for inspection tasks," *J. Intell. Rob. Syst.* **91**, 333–347 (2017).

[3] L. Briones, P. Bustamante and M. Serna, "ROBICEN: A wall-climbing pneumatic robot for inspection in nuclear power plants," *Rob. Comput. Integr. Manuf.* **11**(4), 287–292 (1994).

[4] H. F. Zhu, Y. S. Guan, W. Q. Wu, L. M. Zhang, X. F. Zhou and H. Zhang, "Autonomous pose detection and alignment of suction modules of a biped wall-climbing robot," *IEEE-ASME Trans. Mech.* **20**(2), 653–662 (2015).

[5] T. Yanagida, R. E. Mohan, T. Pathmakumar, K. Elangovan and M. Iwase, "Design and implementation of a shape shifting rolling-crawling-wall-climbing robot," *Appl. Sci. Basel* **7**(4), 342 (2017).

[6] I. M. Koo, T. D. Trong, Y. H. Lee, H. Moon, J. Koo, S. K. Park and H. R. Choi, "Development of wall climbing robot system by using impeller type adhesion mechanism," *J. Intell. Rob. Syst.* **72**(1), 57–72 (2013).

[7] K. Nagaoka, H. Minote, K. Maruya, Y. Shirai, K. Yoshida, T. Hakamada, H. Sawada and T. Kubota, "Passive spine gripper for free-climbing robot in extreme terrain," *IEEE Rob. Autom. Lett.* **3**(3), 1765–1770 (2018).

[8] R. T. Pack, J. L. Christopher and K. Kawamura, "A Rubbertuator-Based Structure-Climbing Inspection Robot," *Proceedings of International Conference on Robotics and Automation,* vol. 1863 (1997) pp. 1869–1874.

[9] K. Nagaya, T. Yoshino, M. Katayama, I. Murakami and Y. Ando, "Wireless piping inspection vehicle using magnetic adsorption force," *IEEE/ASME Trans. Mech.* **17**(3), 472–479 (2012).

[10] W. Fischer, F. Tâche and R. Siegwart, "Magnetic Wall Climbing Robot for Thin Surfaces with Specific Obstacles," *Field and Service Robotics: Results of the 6th International Conference* (C. Laugier and R. Siegwart, eds.) (Springer, Berlin, Heidelberg, 2008) pp. 551–561.

[11] Y. Liu, S. Sun, X. Wu and T. Mei, "A wheeled wall-climbing robot with bio-inspired spine mechanisms," *J. Bionic. Eng.* **12**(1), 17–28 (2015).

[12] K. Autumn, M. Buehler, M. Cutkosky, R. Fearing, R. J. Full, D. Goldman, R. Groff, W. Provancher, A. A. Rizzi, U. Saranli, A. Saunders and D. E. Koditschek, "Robotics in Scansorial Environments," *Defense and Security* (SPIE, 2005) p. 12.

[13] B. He, S. Xu, Y. Zhou and Z. Wang, "Mobility properties analyses of a wall climbing hexapod robot," *J. Mech. Sci. Technol.* **32**(3), 1333–1344 (2018).

[14] M. Sitti and R. S. Fearing, "Synthetic gecko foot-hair micro/nano-structures as dry adhesives," *J. Adhes. Sci. Technol.* **17**(8), 1055–1073 (2003).

[15] B. Yurdumakan, N. R. Raravikar, P. M. Ajayan and A. Dhinojwala, "Synthetic gecko foot-hairs from multiwalled carbon nanotubes," *ChCom* (30), 3799–3801 (2005).

[16] M. Sitti and R. S. Fearing, "Synthetic Gecko Foot-Hair Micro/Nano-Structures for Future Wall-Climbing Robots," *2003 IEEE International Conference on Robotics and Automation* (IEEE, 2003) pp. 1164–1170.

[17] H. K. Raut, A. Baji, H. H. Hariri, H. Parveen, G. S. Soh, H. Y. Low and K. L. Wood, "Gecko-inspired dry adhesive based on micro-nanoscale hierarchical arrays for application in climbing devices ACS," *Appl. Mater. Interfaces* **10**(1), 1288–1296 (2018).

[18] I. H. Han, H. Yi, C. W. Song, H. E. Jeong and S. Y. Lee, "A miniaturized wall-climbing segment robot inspired by caterpillar locomotion," *Bioinspiration Biomim.* **12**(4): 046003 (2017).

[19] A. Peyvandi, P. Soroushian and J. Lu, "A new self-loading locomotion mechanism for wall climbing robots employing biomimetic adhesives," *J. Bionic. Eng.* **10**(1), 12–18 (2013).

[20] Y. Liu, H. Kim and T. Seo, "AnyClimb: A new wall-climbing robotic platform for various curvatures," *IEEE-ASME Trans. Mech.* **21**(4), 1812–1821 (2016).

[21] H. Ko, H. Yi and H. E. Jeong, "Wall and ceiling climbing quadruped robot with superior water repellency manufactured using 3D printing (UNIclimb)," *Int. J. Precision Eng. Manuf. Green Technol.* **4**(3), 273–280 (2017).

[22] K. Autumn, A. Dittmore, D. Santos, M. Spenko and M. Cutkosky, "Frictional adhesion: A new angle on gecko attachment," *J. Exp. Biol.* **209**(18), 3569–3579 (2006).

[23] S. Gorb, M. Varenberg, A. Peressadko and J. Tuma, "Biomimetic mushroom-shaped fibrillar adhesive microstructure," *J. R. Soc. Interface* **4**(13), 271–275 (2007).

[24] Y. Sugizaki, T. Shiina, Y. Tanaka and A. Suzuki, "Effects of peel angle on peel force of adhesive tape from soft adherend," *J. Adhes. Sci. Technol.* **30**(24), 2637–2654 (2016).

[25] K. Kendall, "Thin-film peeling-the elastic term," *J. Phys. D Appl. Phys.* **8**(13), 1449–1452 (1975).

[26] Z. Wang, Z. Dai, Z. Yu and D. Shen, "Optimal Attaching and Detaching Trajectory for Bio-Inspired Climbing Robot Using Dry Adhesive," *IEEE/ASME International Conference on Advanced Intelligent Mechatronics* (2014).

[27] K. Autumn, M. Sitti, Y. A. Liang, A. M. Peattie, W. R. Hansen, S. Sponberg, T. W. Kenny, R. Fearing, J. N. Israelachvili and R. J. Full, "Evidence for van der Waals adhesion in gecko setae," *Proc. Nat. Acad. Sci.* **99**(19), 12252–12256 (2002).